



# Urchin-like hollow-structured cobalt oxides with excellent anode performance for lithium-ion batteries



Chunyu Zhu<sup>\*</sup>, Genki Saito, Tomohiro Akiyama

Center for Advanced Research of Energy & Materials, Hokkaido University, Sapporo 060-8628, Japan

## ARTICLE INFO

### Article history:

Received 27 March 2015

Received in revised form

19 May 2015

Accepted 30 May 2015

Available online 11 June 2015

### Keywords:

Cobalt oxides

Lithium ion battery

Anode material

Hollow structure

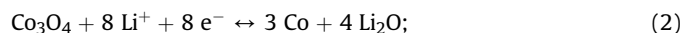
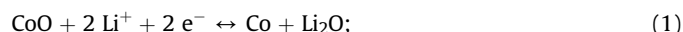
## ABSTRACT

Urchin-like CoO and Co<sub>3</sub>O<sub>4</sub> hollow structures with potential use as anodes in lithium ion batteries were synthesized via the facile thermal decomposition of precipitated amorphous cobalt carbonate hydroxide under either Ar or air. The morphology and, consequently, electrochemical properties of the samples were highly dependent on the precipitation temperature. The cobalt oxides, as derived from precursors that were obtained at room temperature, exhibited superior activity to those obtained at 50 °C and 80 °C because of their unique nanosized architecture. Meanwhile, CoO samples demonstrated much better cyclability and rate capability than Co<sub>3</sub>O<sub>4</sub> samples, as they exhibited much higher coulombic efficiency and lower hysteresis for lithium insertion/extraction. The curved, short, and closely entangled nanowires of CoO sample, which was derived from room temperature precursor, yielded excellent electrochemical performance. The sample displayed a high reversible capacity of about 850 mAh g<sup>-1</sup> at a current density of 500 mA g<sup>-1</sup>, a good stability through 50 cycles with a high coulombic efficiency of about 98%, and a high rate capability of 610 mAh g<sup>-1</sup> even at a rate of 3000 mA g<sup>-1</sup>.

© 2015 Elsevier B.V. All rights reserved.

## 1. Introduction

Current research on negative electrodes for Li-ion batteries (LIBs) is mainly focused on both enhancing the electrochemical performance of commonly used carbonaceous materials through physical and chemical manipulation and finding alternative materials for this application. The first route has been limited by the theoretical capacity of carbonaceous anodes. However, the second approach has led to the discovery of new attractive materials, including Ti-based oxides such as TiO<sub>2</sub> and Li<sub>4</sub>Ti<sub>5</sub>O<sub>12</sub> [1–6], metals or alloys consisted of elements like Sn and Si [7–10], and conversion reaction anode materials such as oxides [11–19], nitrides [20–22], and hydrides [23,24]. Cobalt oxides particularly have been widely studied given their high theoretical capacities. CoO and Co<sub>3</sub>O<sub>4</sub> are the most promising candidates in this class, which theoretically undergo the following reversible reactions:



However, the low capacity retention and poor rate capability underlying the conversion reactions with huge volume changes have restricted their practical application [25,26]. One of the most successful strategies for resolving these problems has been through the fabrication of nanosized structures. A great deal of research have focused on developing materials exhibiting novel morphologies, including nanowires [27,28], nanorods [29], nanoparticles [30], nanosheets [31], and hollow structures [13,26,32]. Generally speaking, hollow microstructures with nanosized subunits and designed voids [13,26,33,34], exhibit especially good electrochemical properties due to the increased mass-electrolyte contact area, shortened Li<sup>+</sup> diffusion distance, and alleviated structural strain that results from repeated lithium insertion-extraction process. Despite significant advancements, it continues to be a challenging issue to improve the rate capacity and cycling stability of cobalt oxide materials.

In this work, we report the simple preparation of urchin-like CoO and Co<sub>3</sub>O<sub>4</sub> hollow structure. Cobalt oxides were synthesized via the thermal decomposition of precipitated amorphous cobalt carbonate hydroxide under Ar or air atmospheres. Unlike previous reports, which have synthesized precursors such as Co(OH)<sub>2</sub>, CoCO<sub>3</sub>, and cobalt carbonate hydroxide under sealed high-pressure conditions

<sup>\*</sup> Corresponding author.

E-mail addresses: [chunyu6zhu@gmail.com](mailto:chunyu6zhu@gmail.com), [chunyu6zhu@eng.hokudai.ac.jp](mailto:chunyu6zhu@eng.hokudai.ac.jp) (C. Zhu).

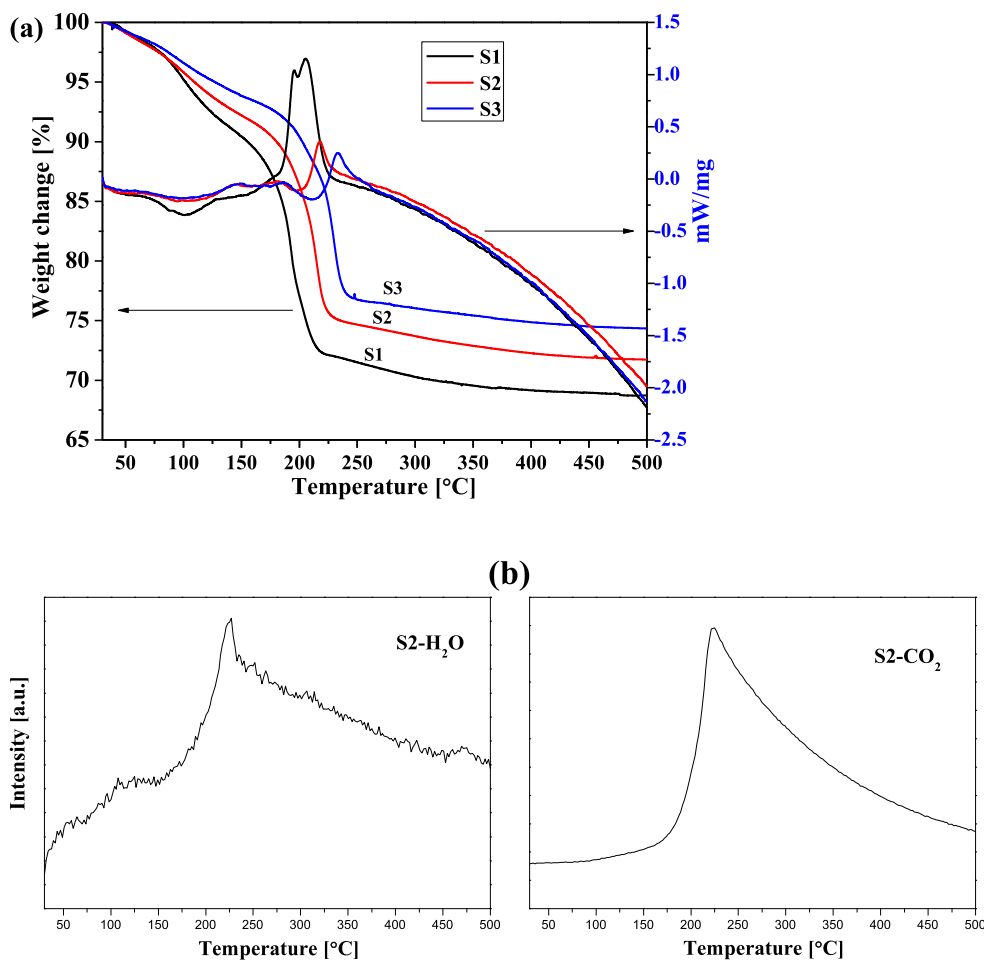


Fig. 1. (a) TG and DSC curves for precursor decomposition under air; (b) MS spectra of water and CO<sub>2</sub> produced as a result of sample decomposition.

and temperatures ranging from 90 to 180 °C [15,31,35–37]. Our procedure employs a scalable precipitation method at/near room temperature. The synthesized cobalt oxide materials show high reversible capacity and superior rate performance.

## 2. Experimental

### 2.1. Preparation of cobalt carbonate hydroxide

Commerically available  $\text{Co}(\text{NO}_3)_2 \cdot 6\text{H}_2\text{O}$ ,  $\text{NH}_4\text{HCO}_3$ , and  $(\text{NH}_4)_2\text{SO}_4$  were used as reagents in the synthesis. First, 20 mmol of  $\text{Co}(\text{NO}_3)_2 \cdot 6\text{H}_2\text{O}$  and 200 mmol of  $(\text{NH}_4)_2\text{SO}_4$  were dissolved in 700 mL of distilled water, yielding solution A. At the same time, 200 mmol of  $\text{NH}_4\text{HCO}_3$  was dissolved in 700 mL of distilled water, forming solution B. Then, 100 mL of ethanol was added to solution A under vigorous stirring, after which solution B was introduced. The resulting mixture was stirred in a water bath for 24 h at room temperature for sample 1 (S1), 50 °C for sample 2 (S2), and 80 °C for sample 3 (S3). The pink precipitates were collected by centrifugation and washed several times with distilled water and ethanol. Finally, the samples were dried at 60 °C over night.

### 2.2. Preparation of cobalt oxides

The precipitates were heated to 500 °C over 2.5 h and kept at this temperature for 3 h under either air or Ar. Heat treatment under air produced  $\text{Co}_3\text{O}_4$ , while treatment under Ar produced  $\text{CoO}$ . The obtained oxides were denoted as S1- $\text{Co}_3\text{O}_4$ , S1- $\text{CoO}$ , S2- $\text{Co}_3\text{O}_4$ , S2- $\text{CoO}$ , S3- $\text{Co}_3\text{O}_4$ , and S3- $\text{CoO}$ , respectively.

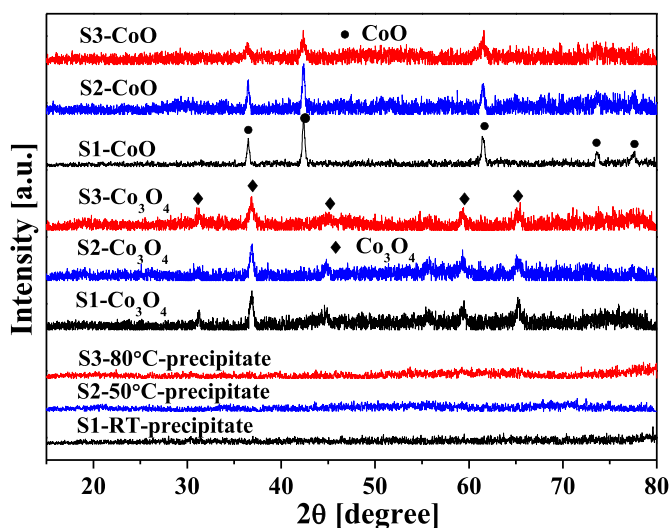
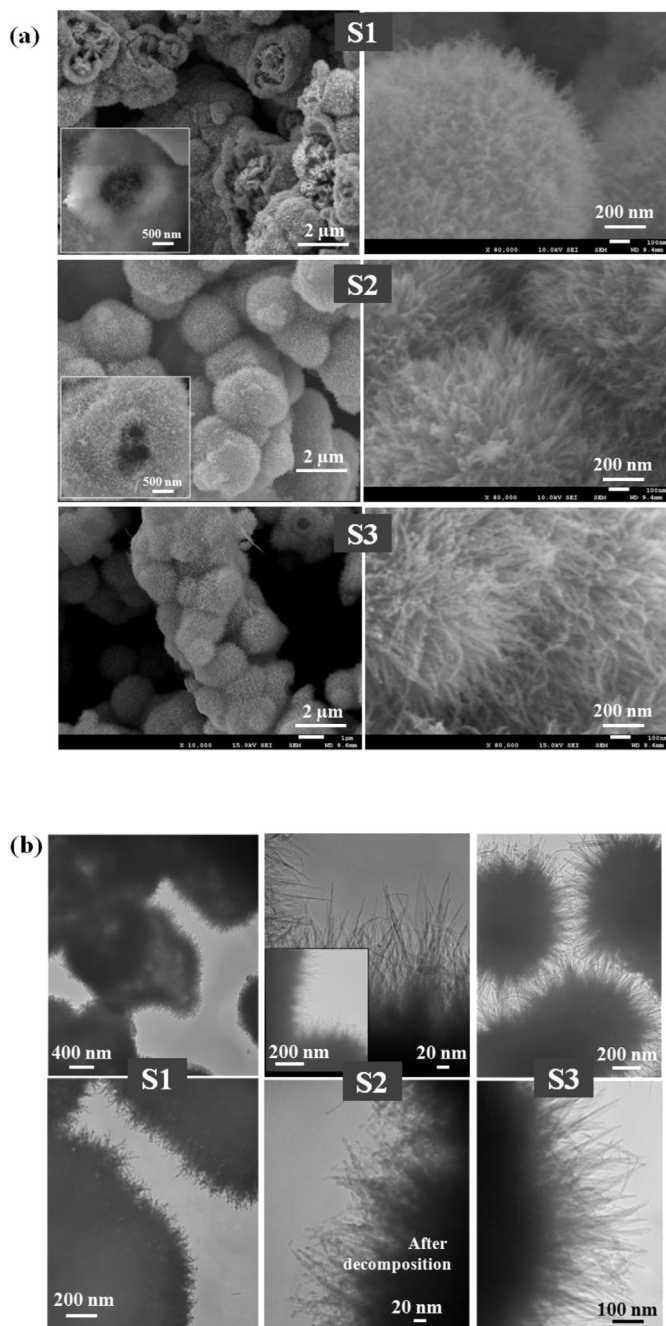


Fig. 2. XRD patterns for the precipitated precursors and cobalt oxide samples.



**Fig. 3.** (a) SEM (b) TEM images of the precipitated samples. A TEM image at a high magnification of the resultant oxide (S2, after decomposition) is also shown as a comparison. Note that the morphology of the precipitated samples and the resultant cobalt oxides is almost the same as observed by SEM or TEM under a low magnification.

### 2.3. Material characterization

Powder X-ray diffraction (XRD, Rigaku Miniflex), scanning electron microscopy (SEM, JEOL, JSM-7400F), and transmission electron microscopy (TEM, JEM-2010F, 200 kV) were used to characterize the phase composition and microscopic morphology. The BET specific surface area was determined by nitrogen sorption using a quantachrome surface area analyzer. Thermogravimetric analysis (TG, Mettler Toledo) and differential scanning calorimetry (DSC) were carried out at a heating rate of  $5^{\circ}\text{C min}^{-1}$  to elucidate

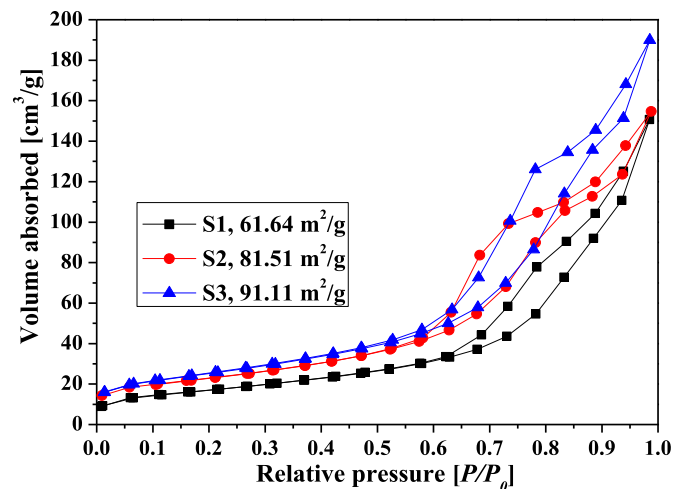


**Fig. 4.** BET  $\text{N}_2$  sorption isotherms for the cobalt oxide samples.

decomposition behavior of the precipitates. A mass spectrometry (MS) was also used to characterize the gases that resulted from decomposition.

### 2.4. Electrochemical measurements

Electrochemical performance was studied using a two-electrode union-joint cell based on a modified Swagelok-type design. The design is shown in Fig. S1 (Supporting Information). A lithium disk was used as both the counter and reference electrode. The working electrode was composed of the cobalt oxides, conductive carbon (acetylene black), and a polyvinylidene fluoride binder, in a weight ratio of 70:20:10. N-methyl-2-pyrrolidone was used as a solvent to produce a slurry of the above materials, which was then coated on a Cu foil current collector. The coated electrodes were dried under vacuum at  $100^{\circ}\text{C}$  over night and cut into 14 mm disks, each of which had a mass of about 3 mg. Cell assembly was carried out in an Ar-filled glove box. A 1 M solution of  $\text{LiPF}_6$  in a 50:50 (v/v) mixture of ethylene carbonate and dimethyl carbonate was used as the electrolyte. Galvanostatic charge/discharge measurements were conducted using an Arbin battery tester with a voltage range of 0.01–3.0 V versus  $\text{Li/Li}^+$  and at a constant temperature of  $25^{\circ}\text{C}$ . Cyclic voltammetry (CV) was performed using a potentiostat/galvanostat apparatus (Autolab, PGSTAT128N) set to a potential scanning rate of  $0.1 \text{ mV s}^{-1}$  and a voltage range of 0.01–3.0 V versus  $\text{Li/Li}^+$ .

## 3. Results and discussion

### 3.1. Structure and morphology

The formation of cobalt carbonate hydroxide,  $\text{CoCO}_3 \cdot \text{Co}(\text{OH})_x \cdot n\text{H}_2\text{O}$ , is described in the following formula:

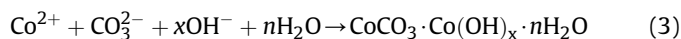


Fig. 1(a) shows the TG and DSC curves for the precipitates, which had been analyzed under an air flow of  $40 \text{ mL min}^{-1}$ . The profiles reveal two stages of weight loss overall. The first drop in weight, which occurred below  $175^{\circ}\text{C}$ , was likely the result of combined water removal, while the second steeper drop above  $175^{\circ}\text{C}$  was resulted from the release of water from hydroxide and  $\text{CO}_2$  from carbonate. The released gas was also confirmed by MS. Fig. 1(b) shows the typical MS spectra of  $\text{H}_2\text{O}$  and  $\text{CO}_2$  gases released during TG measurement.

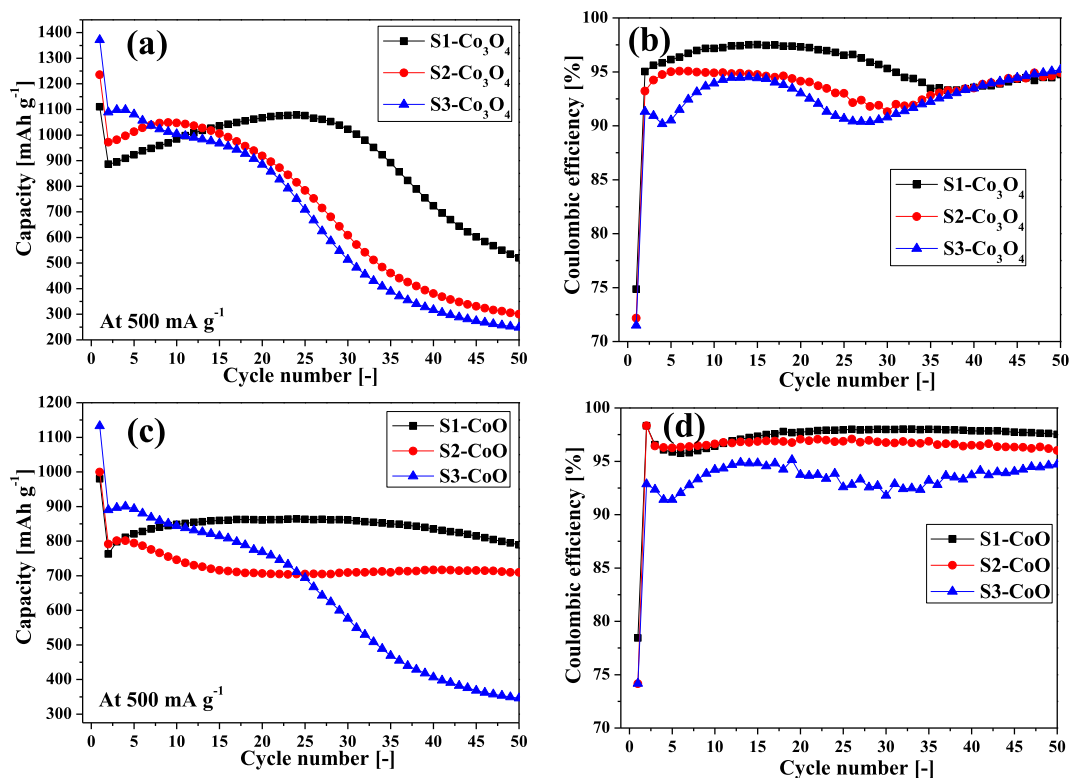
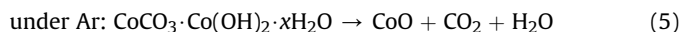
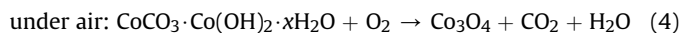


Fig. 5. Electrochemical properties for the cobalt oxide electrodes. (a, c) Cycling performance at a current density of 500 mA g<sup>-1</sup>, and (b, d) the corresponding coulombic efficiencies.

Fig. 2 shows the XRD patterns for both cobalt carbonate hydroxide precursors and the final cobalt oxides. The precipitated precursors are amorphous. The XRD peaks for the samples heated at air atmosphere can be indexed to a phase of Co<sub>3</sub>O<sub>4</sub> (JCPDS no. 42-1467), while the peaks for the samples heated at Ar atmosphere indicate a phase of CoO (JCPDS no. 42-1300). The decomposition reactions can be described by the following formulas:



Sample morphology was assessed using SEM and TEM as shown in Fig. 3 and Fig. S2. The samples presented urchin-like structures. These structures were assembled from individual nanowires with diameters of less than 10 nm. Interestingly, the nanowires extruded outward from a shared hollow shell. The S1 nanowires were curved, short, and closely entangled, while the S2 and S3 nanowires were straight and long. This indicates that the precipitate of cobalt carbonate hydroxide has higher growth rate at elevated solution temperatures. Furthermore, the wires exhibited a pod-like structure in which crystals aggregated after decomposition due to significant gas removal and high-temperature sintering. We measured the specific surface areas for the Co<sub>3</sub>O<sub>4</sub> samples using a N<sub>2</sub> sorption method. The results revealed that the oxides had high BET specific surface areas, with values of 62 m<sup>2</sup> g<sup>-1</sup> for S1, 82 m<sup>2</sup> g<sup>-1</sup> for S2, and 91.11 m<sup>2</sup> g<sup>-1</sup> for S3. Fig. 4 shows the BET sorption isotherms.

### 3.2. Electrochemical properties

Fig. 5 shows the cycling performance of the oxide samples at a current density of 500 mA g<sup>-1</sup>, which were cycled in a voltage range of 0.01–3.0 V versus Li/Li<sup>+</sup>. Fig. 6 presents the

corresponding lithium insertion and extration curves at different cycles. The initial discharge capacities for S1-CoO, S2-CoO, S3-CoO, S1-Co<sub>3</sub>O<sub>4</sub>, S2-Co<sub>3</sub>O<sub>4</sub>, and S3-Co<sub>3</sub>O<sub>4</sub> were 980, 999, 1133, 1110, 1235, and 1372 mAh g<sup>-1</sup>, respectively, all of which were larger than their theoretical values. This is usually due to the irreversible reactions, such as the formation of a solid electrolyte interface layer and solvent decomposition in the electrolyte [15,38]. During the initial few cycles, S3 showed the highest capacity while S1 showed the lowest, illustrating a positive correlation between the activity and specific surface area. Meanwhile, clear voltage plateaus at about 1.0 and 0.7 V for Co<sub>3</sub>O<sub>4</sub> and CoO electrodes, respectively, were observed, corresponding to the reaction between Li and cobalt oxides to form metallic Co and Li<sub>2</sub>O. Although the Co<sub>3</sub>O<sub>4</sub> electrodes showed higher capacities of about 1000 mAh g<sup>-1</sup> for the earlier cycles, degradation occurred rapidly with retained capacities of only 520 mAh g<sup>-1</sup> for S1-Co<sub>3</sub>O<sub>4</sub>, 300 mAh g<sup>-1</sup> for S2-Co<sub>3</sub>O<sub>4</sub>, and 249 mAh g<sup>-1</sup> for S3-Co<sub>3</sub>O<sub>4</sub>, after 50 cycles. On the other hand, S1-CoO and S2-CoO consistently showed values of about 850 and 710 mAh g<sup>-1</sup>, respectively, during the 50 cycles, while S3-CoO continuously lost its capacity after the eighth cycle. Investigation of the coulombic efficiency for lithium deintercalation/intercalation indicated a stable efficiency of around 98% for S1-CoO, and the values decreased in an order of S1-CoO, S2-CoO, S1-Co<sub>3</sub>O<sub>4</sub>, S2-Co<sub>3</sub>O<sub>4</sub>, S3-CoO, and S3-Co<sub>3</sub>O<sub>4</sub>. Table 1 summarizes the typical values of the electrochemical properties. Totally, S1 samples showed better cycling performance than S2 and S3 samples, and CoO electrodes presented better capacity retention efficiency than Co<sub>3</sub>O<sub>4</sub> electrodes. Overall, the large difference in cycling stability can mainly be attributed to their structural differences. The loose structure of the S2 and S3 electrodes likely allowed for only poor contact between each particle, since these samples had straight and long nanowires that extruded outward. After several cycles of discharge and charge,

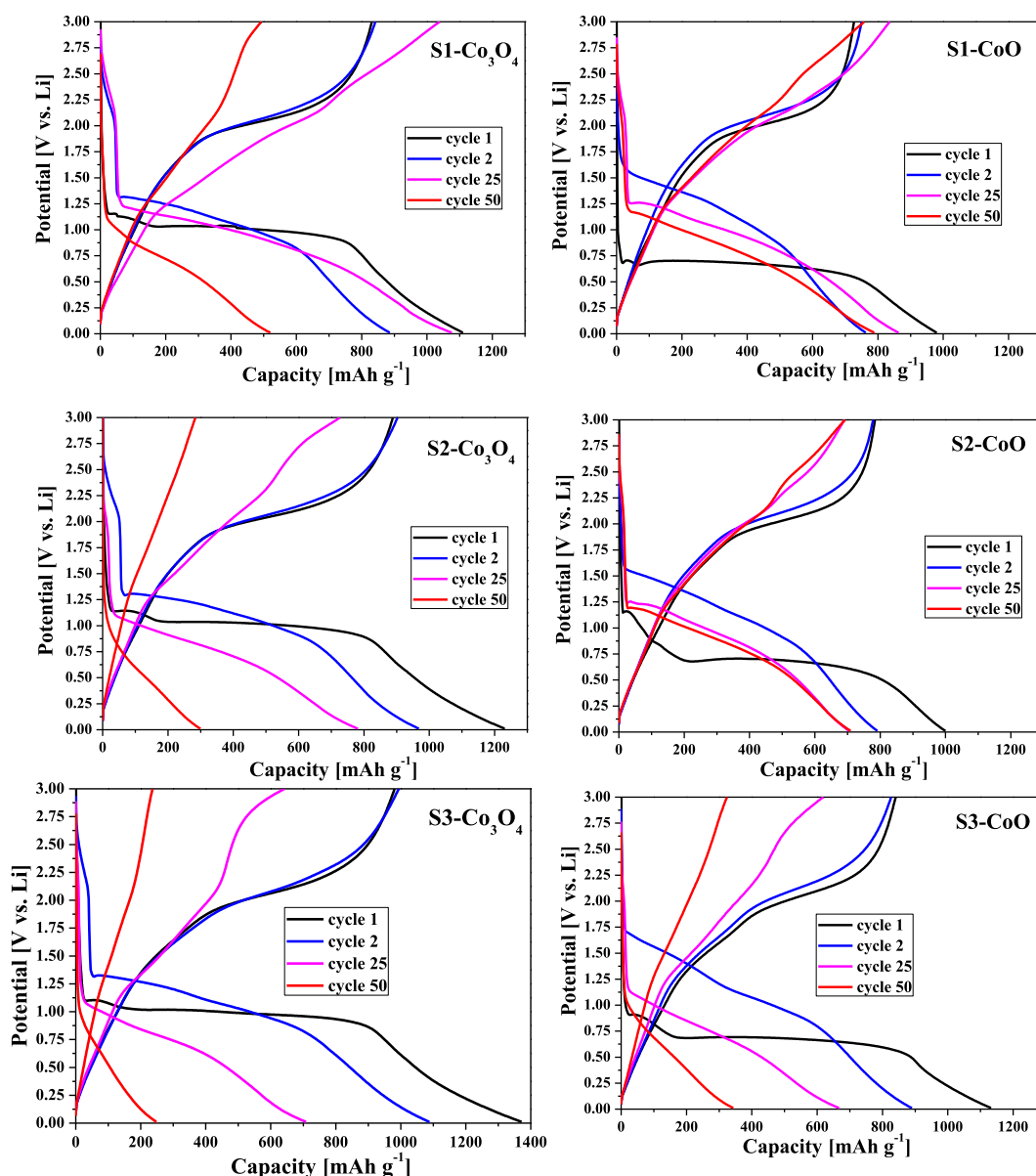


Fig. 6. Discharge/charge curves at different cycles for the cobalt oxide electrodes tested at a current density of  $500 \text{ mA g}^{-1}$ .

the outer wires were pulverized due to the severe volume change, which led to even worse contact between particles. However, the unique structure of S1 with closely entangled nanowires allowed for better contact, at the same time, its structure could maintain necessary voids between each nanosized subunit to alleviate the volume change. Note that the high surface areas of S2 and S3 likely

harmed rather than helped the materials, which increased the potential of side reactions with the electrolyte.

To further investigate the rate capabilities of these samples, current densities were programmed to increase stepwise from  $400$  to  $3000 \text{ mA g}^{-1}$  and finally drop back to  $400 \text{ mA g}^{-1}$ , as shown in Fig. 7. Although the  $\text{Co}_3\text{O}_4$  samples exhibited higher capacities in

Table 1

Cycling performance for the samples at a current density of  $500 \text{ mA g}^{-1}$ .

Sample	$Q_{1st}$ ( $\text{mAh g}^{-1}$ ), charge/discharge; coulombic efficiency	$Q_{max, discharge}$ ( $\text{mAh g}^{-1}$ ), cycle no., and coulombic efficiency	$Q_{50th, discharge}$ ( $\text{mAh g}^{-1}$ )	Capacity retention; $Q_{50th}/Q_{max}$
S1- $\text{Co}_3\text{O}_4$	831.0/1110.2; 74.85%	1078.1; 24th; 96.80%	520.2	48.25%
S2- $\text{Co}_3\text{O}_4$	891.3/1235.3; 72.15%	1048.5; 9th; 94.93%	300.3	28.64%
S3- $\text{Co}_3\text{O}_4$	980.8/1371.8; 71.50%	1098.7; 4th; 90.18%	248.6	22.63%
S1-CoO	726.8/980.1; 78.44%	864.2; 24th; 97.9%	789.4	91.34%
S2-CoO	784.0/999.5; 74.16%	801.4; 4th; 96.30%	709.7	88.56%
S3-CoO	840.1/1132.7; 74.17%	900.4; 4th; 91.41%	346.2	38.45%

$Q_{max, discharge}$  is the peak discharge capacity after the first cycle. Coulombic efficiency is the efficiency for lithium deintercalation/intercalation.



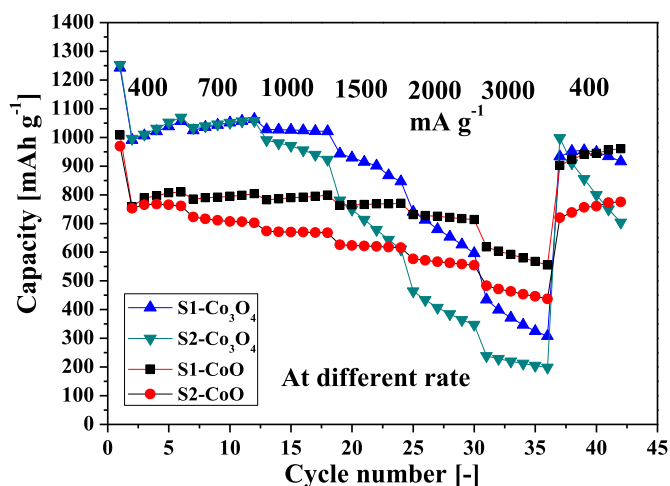


Fig. 7. Cycling performance of S1 and S2 cobalt oxide electrodes at different current densities.

the initial few cycles, CoO electrodes presented better rate capabilities. The S1-CoO electrode showed the best rate capability overall, illustrating a high capacity of  $610 \text{ mAh g}^{-1}$  even at a high rate of  $3000 \text{ mA g}^{-1}$ . However, this increase in current rate adversely affected the capacities for S2-CoO, S1-Co<sub>3</sub>O<sub>4</sub>, and S2-Co<sub>3</sub>O<sub>4</sub>, reducing them to 488, 427, and  $224 \text{ mAh g}^{-1}$  respectively at a rate of  $3000 \text{ mA g}^{-1}$ . Since that S3 samples had presented even worse performance than both S1 and S2 in the tests at a constant current density, they were not analyzed here.

Cyclic voltammetry is also used to analyze the conversion reaction and redox potentials. Fig. 8 shows the CV curves of the 1st to 4th cycles for the electrodes, which were obtained over a voltage range of 0.01–3.0 V and at a potential scan rate of  $0.1 \text{ mV s}^{-1}$ . The observed peaks in CVs closely resemble galvanostatic discharge–charge curves in Fig. 6. The main cathodic peaks correspond to reduction of cobalt oxides to cobalt metal and lithium oxide, while the main anodic peaks represent the formation of cobalt oxide. It can be clearly seen that for all samples, the CV curves of the first cycle are considerably different from those of subsequent cycles. Furthermore, the first CV peaks, especially for

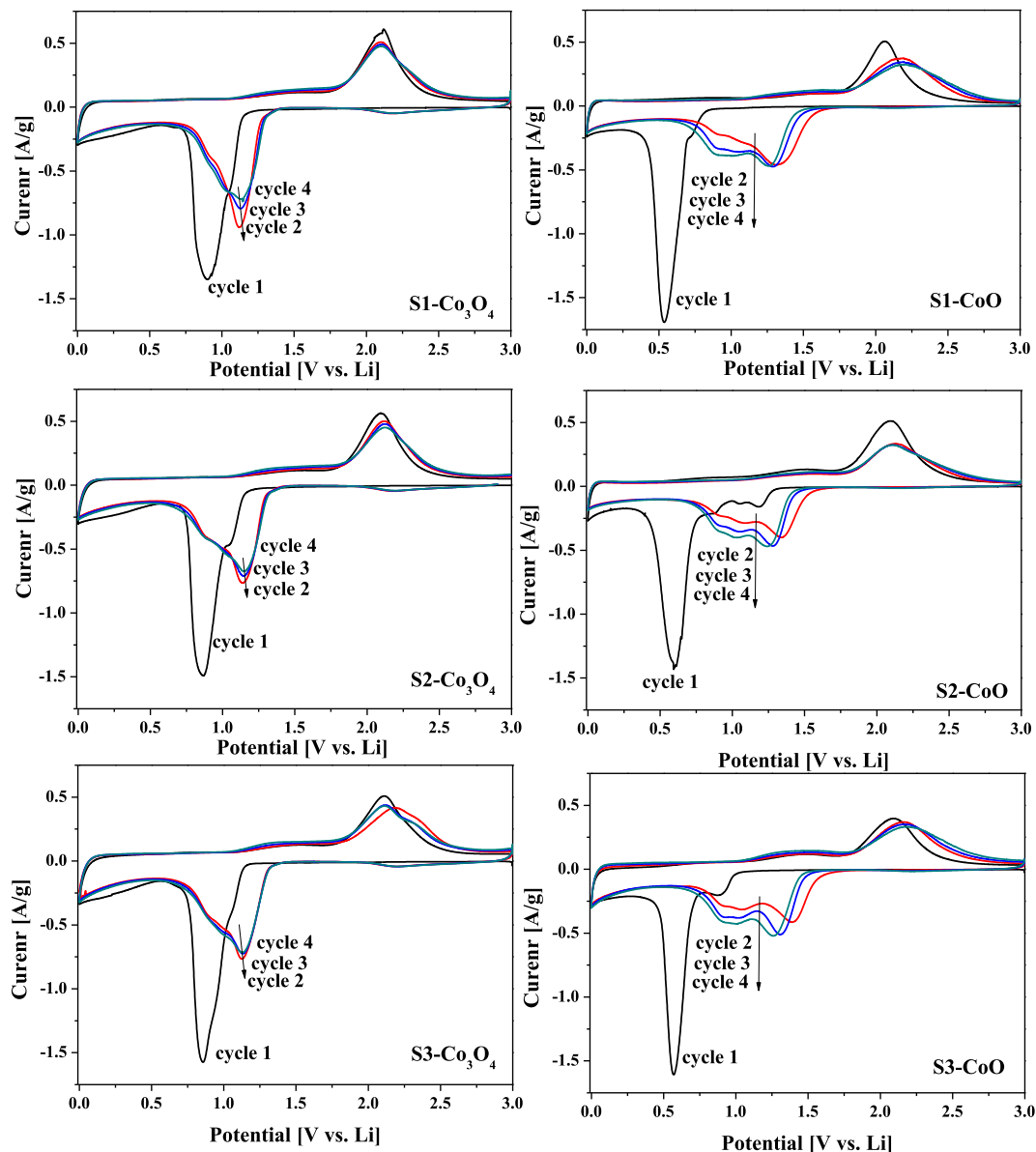


Fig. 8. CV curves for the oxide samples at a potential scan rate of  $0.1 \text{ mV s}^{-1}$ .

the cathodic ones, are significantly different between the  $\text{Co}_3\text{O}_4$  and CoO electrodes.

In the first cycle, cathodic peaks with maximum values at around 0.85 and 0.6 V were observed for the  $\text{Co}_3\text{O}_4$  and CoO electrodes respectively. These two peak potentials also correspond to the dominant voltage plateaus that were observed in the first galvanostatic discharge curves (Fig. 6) at about 1.0 and 0.7 V for  $\text{Co}_3\text{O}_4$  and CoO electrodes, respectively. Here, the voltage differences observed between these two analyses are due to their difference in scanning speeds. Meanwhile, in the opposing delithiation process, similar anodic peaks at around 2.1 V were observed for both the  $\text{Co}_3\text{O}_4$  and CoO electrodes, corresponding to the oxidation of metallic Co to CoO. These anodic peaks also resemble the galvanostatic charge profiles as shown in Fig. 6, illustrating potential plateaus at around 2.1 V.

The reduction peaks shifted positively in the second cycle, moving from 0.85 V to about 1.15 V for the  $\text{Co}_3\text{O}_4$  electrodes and from 0.6 V to about 1.30 V for the CoO electrodes. As compared to the first lithiation process, covered peak areas decreased and were kept almost constant from the second to fourth cycles. While alleviation of the polarization effect has been used to explain the observed shift in potential, oxidation peaks for both  $\text{Co}_3\text{O}_4$  and CoO only showed a small shift, moving from 2.1 V to about 2.11–2.13 V. Apparently, there was greater alleviation of the cathodic/anodic hysteresis of the CoO electrode than for the  $\text{Co}_3\text{O}_4$  electrode after the second cycle; the shortened voltage difference in the discharge/charge measurements further reinforces this conclusion.

#### 4. Conclusions

In summary, novel CoO and  $\text{Co}_3\text{O}_4$  urchin-like hollow structures were prepared by the thermal decomposition of precipitated cobalt carbonate hydroxides under either Ar or air. The cobalt oxides as-derived from the precipitated precursor at room temperature exhibited better electrochemical properties than those precipitated at elevated temperatures due to their unique nanosized architecture. Overall, CoO samples showed much better cyclability and rate capability than  $\text{Co}_3\text{O}_4$  samples because of their much higher coulombic efficiency and lower hysteresis for lithium insertion/extraction. The CoO sample as-derived from the room temperature precursor presented excellent electrochemical performance, showing a high reversible capacity of about  $850 \text{ mAh g}^{-1}$  at a current density of  $500 \text{ mA g}^{-1}$ , a good stability through 50 cycles with a coulombic efficiency of about 98%, and a high rate capability indicating a capacity of  $610 \text{ mAh g}^{-1}$  even at a rate of  $3000 \text{ mA g}^{-1}$ . These cobalt oxides could potentially be applied as high capacity anode materials for LIBs, with other potential applications in gas sensors, supercapacitors, and catalysts as well.

#### Acknowledgments

This work was financially supported partially by the Japan Society for Promotion of Science (JSPS) and Japan Science and Technology Agency (JST).

#### Appendix A. Supplementary data

Supplementary data related to this article can be found at <http://dx.doi.org/10.1016/j.jallcom.2015.05.206>.

#### References

- [1] L. Yu, H.B. Wu, X.W. Lou, Mesoporous  $\text{Li}_4\text{Ti}_5\text{O}_{12}$  hollow spheres with enhanced lithium storage capability, *Adv. Mater.* 25 (2013) 2296–2300.
- [2] K. Zhu, J. Tian, Y. Liu, N. Lin, Q. Tang, X. Yu, Y. Zhu, Z. Shan, Submicron-sized mesoporous anatase  $\text{TiO}_2$  beads with a high specific surface synthesized by controlling reaction conditions for high-performance Li-batteries, *RSC Adv.* 3 (2013) 13149–13155.
- [3] Z. Zhu, F. Cheng, J. Chen, Investigation of effects of carbon coating on the electrochemical performance of  $\text{Li}_4\text{Ti}_5\text{O}_{12}/\text{C}$  nanocomposites, *J. Mater. Chem. A* 1 (2013) 9484–9490.
- [4] X. Li, H. Hu, S. Huang, G. Yu, L. Gao, H. Liu, Y. Yu, Nano-sized  $\text{Li}_4\text{Ti}_5\text{O}_{12}$  anode material with excellent performance prepared by solid state reaction: the effect of precursor size and morphology, *Electrochim. Acta* 112 (2013) 356–363.
- [5] Z. Yan, L. Liu, H. Guo, J. Tan, H. Shu, X. Yang, H. Hu, Q. Zhou, Z. Huang, X. Wang, One-pot synthesis of FCNTs-wired  $\text{TiO}_2$  nanocomposites as anode materials for high-rate lithium ion batteries, *Electrochim. Acta* 123 (2014) 551–559.
- [6] F. Li, P. Chen, H. Wu, Y. Zhang, Cooperative enhancement of electrochemical properties in double carbon-decorated  $\text{Li}_4\text{Ti}_5\text{O}_{12}/\text{C}$  composite as anode for Li-ion batteries, *J. Alloys Compd.* 633 (2015) 443–447.
- [7] G. Saito, C. Zhu, T. Akiyama, Surfactant-assisted synthesis of Sn nanoparticles via solution plasma technique, *Adv. Powder Technol.* 25 (2014) 728–732.
- [8] Z. Tan, Z. Sun, H. Wang, Q. Guo, D. Su, Fabrication of porous Sn-C composites with high initial coulomb efficiency and good cyclic performance for lithium ion batteries, *J. Mater. Chem. A* 1 (2013) 9462–9468.
- [9] Y. Zhao, X. Liu, H. Li, T. Zhai, H. Zhou, Hierarchical micro/nano porous silicon Li-ion battery anodes, *Chem. Commun.* 48 (2012) 5079–5081.
- [10] M. Zhang, X. Hou, J. Wang, M. Li, S. Hu, Z. Shao, X. Liu, Interweaved Si/C/CNTs/CNFs composites as anode materials for Li-ion batteries, *J. Alloys Compd.* 588 (2014) 206–211.
- [11] L. Wang, J. Liang, Y. Zhu, T. Mei, X. Zhang, Q. Yang, Y. Qian, Synthesis of  $\text{Fe}_3\text{O}_4@C$  core-shell nanorings and their enhanced electrochemical performance for lithium-ion batteries, *Nanoscale* 5 (2013) 3627–3631.
- [12] L. Wang, Y. Li, Z. Han, L. Chen, B. Qian, X. Jiang, J. Pinto, G. Yang, Composite structure and properties of  $\text{Mn}_3\text{O}_4/\text{graphene}$  oxide and  $\text{Mn}_3\text{O}_4/\text{graphene}$ , *J. Mater. Chem. A* 1 (2013) 8385–8397.
- [13] J. Wang, N. Yang, H. Tang, Z. Dong, Q. Jin, M. Yang, D. Kisailus, H. Zhao, Z. Tang, D. Wang, Accurate control of multishelled  $\text{Co}_3\text{O}_4$  hollow microspheres as high-performance anode materials in lithium-ion batteries, *Angew. Chem.* 125 (2013) 6545–6548.
- [14] Q. Hao, M. Li, S. Jia, X. Zhao, C. Xu, Controllable preparation of  $\text{Co}_3\text{O}_4$  nanosheets and their electrochemical performance for Li-ion batteries, *RSC Adv.* 3 (2013) 7850–7854.
- [15] S.-W. Bian, L. Zhu, Template-free synthesis of mesoporous  $\text{Co}_3\text{O}_4$  with controlled morphologies for lithium ion batteries, *RSC Adv.* 3 (2013) 4212–4215.
- [16] Y. Yu, Y. Zhu, J. Liang, L. fan, Y. Qian, Synthesis of a novel carbon network-supported  $\text{Fe}_3\text{O}_4@C$  composite and its applications in high-power lithium-ion batteries, *Electrochimica Acta* 111 (2013) 809–813.
- [17] S.-K. Park, A. Jin, S.-H. Yu, J. Ha, B. Jang, S. Bong, S. Woo, Y.-E. Sung, Y. Piao, In situ hydrothermal synthesis of  $\text{Mn}_3\text{O}_4$  nanoparticles on nitrogen-doped graphene as high-performance anode materials for lithium ion batteries, *Electrochimica Acta* 120 (2014) 452–459.
- [18] C. Zhu, G. Saito, T. Akiyama, A facile solution combustion synthesis of nano-sized amorphous iron oxide incorporated in a carbon matrix for use as a high-performance lithium ion battery anode material, *J. Alloys Compd.* 633 (2015) 424–429.
- [19] N. Sivakumar, S.R.P. Gnanakan, K. Karthikeyan, S. Amareesh, W.S. Yoon, G.J. Park, Y.S. Lee, Nanostructured  $\text{MgFe}_2\text{O}_4$  as anode materials for lithium-ion batteries, *J. Alloys Compd.* 509 (2011) 7038–7041.
- [20] X. Li, M.M. Hasan, A.L. Hector, J.R. Owen, Performance of nanocrystalline  $\text{Ni}_3\text{N}$  as a negative electrode for sodium-ion batteries, *J. Mater. Chem. A* 1 (2013) 6441–6445.
- [21] B. Das, M.V. Reddy, G.V.S. Rao, B.V.R. Chowdari, Synthesis of porous-CoN nanoparticles and their application as a high capacity anode for lithium-ion batteries, *J. Mater. Chem.* 22 (2012) 17505–17510.
- [22] B. Das, M.V. Reddy, G.V. Subba Rao, B.V.R. Chowdari, Synthesis and Li-storage behavior of CrN nanoparticles, *RSC Adv.* 2 (2012) 9022–9028.
- [23] Y. Oumellal, A. Rougier, J.M. Tarascon, L. Aymard,  $2\text{LiH} + \text{M}$  (M = Mg, Ti): new concept of negative electrode for rechargeable lithium-ion batteries, *J. Power Sources* 192 (2009) 698–702.
- [24] Y. Oumellal, A. Rougier, G.A. Nazri, J.M. Tarascon, L. Aymard, Metal hydrides for lithium-ion batteries, *Nat. Mater.* 7 (2008) 916–921.
- [25] M.V. Reddy, G.V. Subba Rao, B.V.R. Chowdari, Metal oxides and oxysalts as anode materials for Li ion batteries, *Chem. Rev.* 113 (2013) 5364–5457.
- [26] Z. Wang, L. Zhou, X.W. Lou, Metal oxide hollow nanostructures for lithium-ion batteries, *Adv. Mater.* 24 (2012) 1903–1911.
- [27] F. Zhang, C. Yuan, X. Lu, L. Zhang, Q. Che, X. Zhang, Facile growth of mesoporous  $\text{Co}_3\text{O}_4$  nanowire arrays on Ni foam for high performance electrochemical capacitors, *J. Power Sources* 203 (2012) 250–256.
- [28] J. Chen, X.-h. Xia, J.-p. Tu, Q.-q. Xiong, Y.-X. Yu, X.-l. Wang, C.-d. Gu,  $\text{Co}_3\text{O}_4\text{-C}$  core-shell nanowire array as an advanced anode material for lithium ion batteries, *J. Mater. Chem.* 22 (2012) 15056–15061.
- [29] W. Mei, J. Huang, L. Zhu, Z. Ye, Y. Mai, J. Tu, Synthesis of porous rhombus-shaped  $\text{Co}_3\text{O}_4$  nanorod arrays grown directly on a nickel substrate with high electrochemical performance, *J. Mater. Chem.* 22 (2012) 9315–9321.
- [30] B.G. Choi, S.-J. Chang, Y.B. Lee, J.S. Bae, H.J. Kim, Y.S. Huh, 3D heterostructured architectures of  $\text{Co}_3\text{O}_4$  nanoparticles deposited on porous graphene surfaces for high performance of lithium ion batteries, *Nanoscale* 4 (2012) 5924–5930.

- [31] X. Wang, H. Guan, S. Chen, H. Li, T. Zhai, D. Tang, Y. Bando, D. Golberg, Self-stacked  $\text{Co}_3\text{O}_4$  nanosheets for high-performance lithium ion batteries, *Chem. Commun.* 47 (2011) 12280–12282.
- [32] M.Y. Son, Y.J. Hong, Y.C. Kang, Superior electrochemical properties of  $\text{Co}_3\text{O}_4$  yolk-shell powders with a filled core and multishells prepared by a one-pot spray pyrolysis, *Chem. Commun.* 49 (2013) 5678–5680.
- [33] C. Zhu, G. Saito, T. Akiyama, A new  $\text{CaCO}_3$ -template method to synthesize nanoporous manganese oxide hollow structures and their transformation to high-performance  $\text{LiMn}_2\text{O}_4$  cathodes for lithium-ion batteries, *J. Mater. Chem. A* 1 (2013) 7077–7082.
- [34] C. Zhu, T. Akiyama, Designed synthesis of  $\text{LiNi}_{0.5}\text{Mn}_{1.5}\text{O}_4$  hollow microspheres with superior electrochemical properties as high-voltage cathode materials for lithium-ion batteries, *RSC Adv.* 4 (2014) 10151–10156.
- [35] Y. Fu, X. Li, X. Sun, X. Wang, D. Liu, D. He, Self-supporting  $\text{Co}_3\text{O}_4$  with lemongrass-like morphology as a high-performance anode material for lithium ion batteries, *J. Mater. Chem.* 22 (2012) 17429–17431.
- [36] Y. Wang, H.J. Zhang, L. Lu, L.P. Stubbs, C.C. Wong, J. Lin, Designed functional systems from peapod-like  $\text{Co@carbon}$  to  $\text{Co}_3\text{O}_4\text{@carbon}$  nanocomposites, *ACS Nano* 4 (2010) 4753–4761.
- [37] S. Xiong, J.S. Chen, X.W. Lou, H.C. Zeng, Mesoporous  $\text{Co}_3\text{O}_4$  and  $\text{CoO@C}$  topotactically transformed from chrysanthemum-like  $\text{Co}(\text{CO}_3)0.5(\text{OH})\cdot 0.11\text{H}_2\text{O}$  and their lithium-storage properties, *Adv. Funct. Mater.* 22 (2012) 861–871.
- [38] L. Jin, X. Li, H. Ming, H. Wang, Z. Jia, Y. Fu, J. Adkins, Q. Zhou, J. Zheng, Hydrothermal synthesis of  $\text{Co}_3\text{O}_4$  with different morphologies towards efficient Li-ion storage, *RSC Adv.* 4 (2014) 6083–6089.